Molecular Crystals and Liquid Crystals
Publication details, including instructions for authors and subscription information:
http://www.tandfonline.com/loi/gmcl20

# Some Peculiarities of the Recording of Polarization Diffraction Gratings by Doubling Method

H. L. Margaryan [a], V. M. Aroutiounian [a], D. L. Hovhannisyan [a], N. H. Hakobyan [a] & V. K. Abrahamyan [a]
[a] Yerevan State University, Yerevan, Armenia
Version of record first published: 11 May 2012.

To cite this article: H. L. Margaryan , V. M. Aroutiounian , D. L. Hovhannisyan , N. H. Hakobyan & V. K. Abrahamyan (2012): Some Peculiarities of the Recording of Polarization Diffraction Gratings by Doubling Method, Molecular Crystals and Liquid Crystals, 559:1, 214-227

To link to this article: http://dx.doi.org/10.1080/15421406.2012.661943

*Mol. Cryst. Liq. Cryst.*, Vol. 559: pp. 214–227, 2012

ISSN: 1542-1406 print/1563-5287 online
DOI: 10.1080/15421406.2012.661943



# Some Peculiarities of the Recording of Polarization Diffraction Gratings by Doubling Method

H. L. MARGARYAN,* V. M. AROUTIOUNIAN,
D. L. HOVHANNISYAN, N. H. HAKOBYAN,
AND V. K. ABRAHAMYAN

Yerevan State University, Yerevan, Armenia



*We investigated the dependence of angular dispersion of replica on its distance from the master polarization diffraction grating (PDG). The distribution of field diffracted on master PDG was calculated using the method of finite-difference time-domain. According to the numerical model, within the transition region, conditioned by interference of secondary waves with the same polarization state, the angular dispersion of replica changes depending on the distance between master and replica. Outside the transition region, the angular dispersions of replica and master completely coincide. The experimental investigation was also carried out, the results of which are in good agreement with the calculated data.*

**Keywords** Diffraction efficiency; master PDG; polarization diffraction gratings; printing method; replica

## Introduction

Liquid Crystal Polarization Gratings (LC PDGs) are diffractive optical elements with an anisotropic periodic index profile. Although the polarization gratings are "thin" gratings, the thin-screen approximation predicts high diffraction into the first diffraction orders making them attractive for optical devices. There have numerous applications in photonic systems and displays, including highly efficient projection displays, wide-viewing and direct-view displays, polarized beam splitting devices, multiplexing, and polarization dispersion applications. The unique properties of the polarization gratings are the polarization selectivity of the diffraction efficiency and the capability of these gratings to convert the polarization states of diffraction beams [1–6].

In the recent years, due to the synthesis of new photo-polymerized polymers, the recording of polarization diffraction gratings has become possible. The fabrication of LC polymer PDGs is a multistep process, and each step must be optimized to obtain high-quality PDGs. Recently developed technology for printing PDGs from a master one paves the way to the large-scale production of large area gratings, maintaining the high quality and avoiding all the complexity, cost and stability issues of holographic setups [7].

The printing technique makes use of the rotating polarization pattern obtained at the output of the master PDG from a linearly or circularly polarized input beam. For the "thin"

*Address correspondence to H. L. Margaryan, Faculty of Radiophysics, Yerevan State University, 1 A. Manoogian Str., Yerevan 0025, Armenia. Tel./Fax: + 374 10 578373. E-mail: marhakob@ysu.am

PDGs the regular interference pattern (interferogram) is formed not right at the output of PDG, but at certain distance beyond it. Since, in the printing method, the pattern recording occurs as a result of photopolymerization caused by the field of light diffracted on the master PDG, we assume that quality of the grating in print depends on the distance between master and replica.

In this paper we present the results of theoretical and experimental studies of the PDGs recording process by printing method. We investigated the distribution of the diffracted field at the output of master PDG and the dependence of angular dispersion of replica on its distance from master PDG.



## Numerical Modeling of Electrical Field Distribution at the Output of Master PDG

The analytical description of diffracted field distribution uses approximations, making it impossible to obtain the precise pattern of the field distribution immediately at the output of PDG. For this reason, for theoretical analysis of electrical field distribution at the output of master PDG we use the finite-difference time-domain (FDTD) method. FDTD methods present a robust and powerful approach for directly solving Maxwell's curl equations both in time and space, and are widely used for PDG numerical modeling [8]. Another advantage of FDTD techniques is their capability to visualize real-time pictures of the electromagnetic wave.

In this section the numerical analysis of light propagation through the PDG is presented. Let us consider the case when a linearly polarized beam of a continuous-wave laser $(0, E_y, 0)$ propagates along $z$axis and hits a PDG (the problem's geometry is presented on Fig. 1).

The grating is placed in a position where the LC's director's periodic change occurs in the $x$ axis, let's designate the grating's half-period as $\Lambda$, and the thickness as $L$. At the output of the grating the arrows show the propagation of radiation in $-1$ and $+1$ diffracted orders with left and right circular polarization.

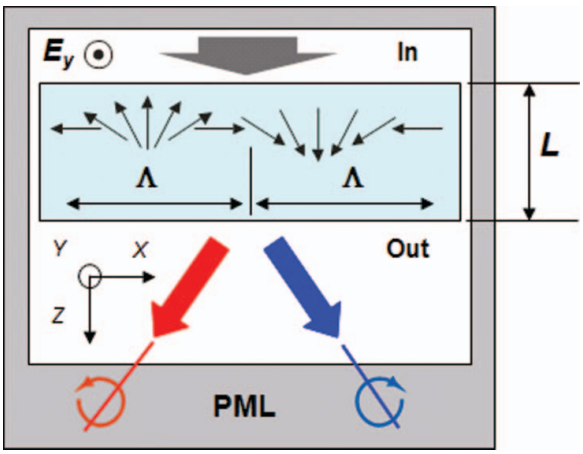


**Figure 1.** The schematic of PDG arrangement with respect to the coordinate axes.

Generally Maxwell's equations for a periodic anisotropic medium can be written as follows:

$$\begin{cases} \dfrac{\partial D_x}{\partial t} = \dfrac{\partial H_z}{\partial y} - \dfrac{\partial H_y}{\partial z} \\ \dfrac{\partial D_y}{\partial t} = \dfrac{\partial H_x}{\partial z} - \dfrac{\partial H_z}{\partial x} \\ \dfrac{\partial D_z}{\partial t} = \dfrac{\partial H_y}{\partial x} - \dfrac{\partial H_x}{\partial y} \end{cases} \tag{1}$$

$$\begin{cases} \dfrac{\partial H_x}{\partial t} = -\dfrac{1}{\mu}\left(\dfrac{\partial E_z}{\partial y} - \dfrac{\partial E_y}{\partial z}\right) \\ \dfrac{\partial H_y}{\partial t} = -\dfrac{1}{\mu}\left(\dfrac{\partial E_x}{\partial z} - \dfrac{\partial E_z}{\partial x}\right) \\ \dfrac{\partial H_z}{\partial t} = -\dfrac{1}{\mu}\left(\dfrac{\partial E_y}{\partial x} - \dfrac{\partial E_x}{\partial y}\right) \end{cases}, \tag{2}$$

where $D_{x,y,z}$ are the electrical induction components, $H_{x,y,z}$ are the magnetic field components, and $\mu$ is permeability of free space. The electric field vector can be described as $E = \tilde{\varepsilon}^{-1} D$ where $\tilde{\varepsilon}$ is a permittivity tensor for a periodic anisotropic medium

$$\varepsilon(\varphi) = \begin{pmatrix} \varepsilon_e \cos^2(\varphi) + \varepsilon_o \sin^2(\varphi) & \Delta\varepsilon \sin(\varphi)\cos(\varphi) & 0 \\ \Delta\varepsilon \sin(\varphi)\cos(\varphi) & \varepsilon_o \cos^2(\varphi) + \varepsilon_e \sin^2(\varphi) & 0 \\ 0 & 0 & \varepsilon_e \end{pmatrix}, \tag{3}$$

where $\varepsilon_{e,}\varepsilon_o$ are dielectric constants for extraordinary and ordinary waves, $\Delta\varepsilon = \varepsilon_e - \varepsilon_o$, LC molecule orientation related angles $\varphi = \pi x/\Lambda, \alpha$. The laboratory axis is shown in Fig. 2.

According to (3), we consider the case when $\alpha = 0$. The components of the electric field vector can be described as

$$\begin{aligned} E_x &= \tilde{\varepsilon}_{xx}^{-1} D_x + \tilde{\varepsilon}_{xy}^{-1} D_y + \tilde{\varepsilon}_{xz}^{-1} D_z, \\ E_y &= \tilde{\varepsilon}_{xy}^{-1} D_x + \tilde{\varepsilon}_{yy}^{-1} D_y + \tilde{\varepsilon}_{yz}^{-1} D_z, \\ E_z &= \tilde{\varepsilon}_{xz}^{-1} D_x + \tilde{\varepsilon}_{yz}^{-1} D_y + \tilde{\varepsilon}_{zz}^{-1} D_z, \end{aligned} \tag{4}$$

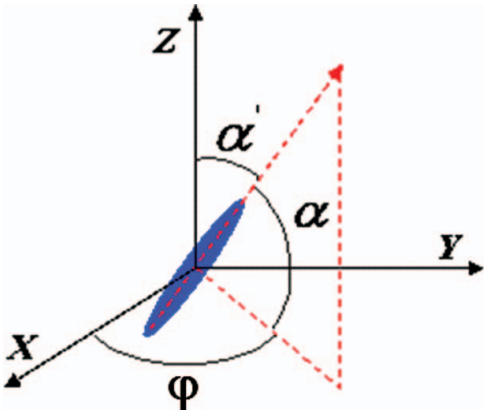


**Figure 2.** LC molecule orientation in laboratory system of coordinates.

where the $\tilde{\varepsilon}_{xx}^{-1}, \varepsilon_{xy}^{-1}, \tilde{\varepsilon}_{xz}^{-1}, \tilde{\varepsilon}_{xy}^{-1}, \tilde{\varepsilon}_{yy}^{-1}, \tilde{\varepsilon}_{yz}^{-1}, \tilde{\varepsilon}_{xz}^{-1}, \tilde{\varepsilon}_{yz}^{-1}, \tilde{\varepsilon}_{zz}^{-1}$ are the components related to the permittivity inverse tensor.

The essential feature in FDTD methods is a proper absorbing boundary condition to truncate the simulation space without artificial reflections. In this section, we used the perfectly matched layer (PML, see Fig. 1) introduced by Berenger [9, 10]. Although at the gratings input we have the linearly-polarized radiation $(0, E_y, 0)$, the anisotropy of the grating also causes the formation of $E_x$ and $E_z$ field components according to (4). To calculate the diffracted field, we make a transition from the continuous space $(x, y, z, t)$ to the discrete one $(i\Delta x, j\Delta y, k\Delta z, \Delta t)$, where $i, j, k, n$ are integer constants. During the first simulation, the electrical induction components were calculated according to (1), whose finite-difference scheme is presented below:

$$\begin{cases} D_x^{n+1/2}\left(i, j+\frac{1}{2}, k+\frac{1}{2}\right) = D_x^{n-1/2}\left(i, j+\frac{1}{2}, k+\frac{1}{2}\right) \\ \quad + \frac{\Delta t}{\Delta y}\left[H_z^n\left(i, j+1, k+\frac{1}{2}\right) - H_z^n\left(i, j, k+\frac{1}{2}\right)\right] \\ \quad - \frac{\Delta t}{\Delta z}\left[H_y^n\left(i, j+\frac{1}{2}, k+1\right) - H_y^n\left(i, j+\frac{1}{2}, k+\frac{1}{2}\right)\right] \\ D_y^{n+1/2}\left(i-\frac{1}{2}, j+1, k+\frac{1}{2}\right) = D_y^{n-1/2}\left(i-\frac{1}{2}, j+1, k+\frac{1}{2}\right) \\ \quad + \frac{\Delta t}{\Delta z}\left[H_x^n\left(i-\frac{1}{2}, j+1, k+1\right) - H_x^n\left(i-\frac{1}{2}, j+1, k\right)\right] \\ \quad - \frac{\Delta t}{\Delta x}\left[H_z^n\left(i, j+1, k+\frac{1}{2}\right) - H_z^n\left(i-1, j+1, k+\frac{1}{2}\right)\right] \\ D_z^{n+1/2}\left(i-\frac{1}{2}, j+\frac{1}{2}, k+1\right) = D_z^{n-1/2}\left(i-\frac{1}{2}, j+\frac{1}{2}, k+1\right) \\ \quad + \frac{\Delta t}{\Delta x}\left[H_y^n\left(i, j+\frac{1}{2}, k+1\right) - H_y^n\left(i-1, j+\frac{1}{2}, k+1\right)\right] \\ \quad - \frac{\Delta t}{\Delta y}\left[H_x^n\left(i-\frac{1}{2}, j+1, k+1\right) - H_x^n\left(i-\frac{1}{2}, j, k+1\right)\right] \end{cases} \tag{5}$$

where $\Delta x = \Delta y = \Delta z = \lambda_0/40$ are the grid space, $\Delta t = \Delta x/2c$ is the time step, $c$ is light velocity in vacuum, $\lambda_0$ is the radiation wavelength, which for the simulation is considered equal to 325 nm. After taking into account that

$$\begin{aligned} \tilde{\varepsilon}_{xx}^{-1} &= \lfloor \varepsilon_o \cos^2(\varphi) + \varepsilon_e \sin^2(\varphi) \rfloor / \varepsilon_o \varepsilon_e, \\ \tilde{\varepsilon}_{xy}^{-1} &= \tilde{\varepsilon}_{yx}^{-1} = [-(\varepsilon_e - \varepsilon_o)\cos(\varphi)\sin(\varphi)]/\varepsilon_o\varepsilon_e \\ \tilde{\varepsilon}_{yy}^{-1} &= [\varepsilon_e \cos^2(\varphi) + \varepsilon_o \sin^2(\varphi)]/\varepsilon_o\varepsilon_e, \tilde{\varepsilon}_{zz}^{-1} = 1/\varepsilon_e \end{aligned} \tag{6}$$

we calculate the electric field components according to (4)

$$\begin{aligned} E_x^n(i, j, k) &= \tilde{\varepsilon}_{xx}^{-1}(i, j, k) D_x^n(i, j, k) + \tilde{\varepsilon}_{xy}^{-1}(i, j, k) D_y^n(i, j, k), \\ E_y^n(i, j, k) &= \tilde{\varepsilon}_{xy}^{-1}(i, j, k) D_x^n(i, j, k) + \tilde{\varepsilon}_{yy}^{-1}(i, j, k) D_y^n(i, j, k), \\ E_z^n(i, j, k) &= \tilde{\varepsilon}_{zz}^{-1}(i, j, k) D_z^n(i, j, k). \end{aligned} \tag{7}$$

At last, with updated values of the electrical field components, we calculated the same ones for magnetic field as presented below:

$$
\begin{cases}
H_x^{n+1}\left(i-\frac{1}{2},j+1,k+1\right)=H_x^{n}\left(i-\frac{1}{2},j+1,k+1\right)\\
\quad+\frac{\Delta t}{\Delta z}\left[E_y^{n+1/2}\left(i-\frac{1}{2},j+1,k+\frac{3}{2}\right)-E_y^{n+1/2}\left(i-\frac{1}{2},j+1,k+\frac{1}{2}\right)\right]\\
\quad-\frac{\Delta t}{\Delta y}\left[E_z^{n+1/2}\left(i-\frac{1}{2},j+\frac{3}{2},k+1\right)-E_z^{n+1/2}\left(i-\frac{1}{2},j+\frac{1}{2},k+1\right)\right]\\
H_y^{n+1}\left(i,j+\frac{1}{2},k+1\right)=H_y^{n}\left(i,j+\frac{1}{2},k+1\right)\\
\quad+\frac{\Delta t}{\Delta x}\left[E_z^{n+1/2}\left(i+\frac{1}{2},j+\frac{1}{2},k+1\right)-E_z^{n+1/2}\left(i-\frac{1}{2},j+\frac{1}{2},k+1\right)\right]\\
\quad-\frac{\Delta t}{\Delta z}\left[E_x^{n+1/2}\left(i,j+\frac{1}{2},k+\frac{3}{2}\right)-E_x^{n+1/2}\left(i,j+\frac{1}{2},k+\frac{1}{2}\right)\right]\\
H_z^{n+1}\left(i,j+1,k+\frac{1}{2}\right)=H_z^{n}\left(i,j+1,k+\frac{1}{2}\right)\\
\quad+\frac{\Delta t}{\Delta y}\left[E_x^{n+1/2}\left(i,j+\frac{3}{2},k+\frac{1}{2}\right)-E_x^{n+1/2}\left(i,j+\frac{1}{2},k+\frac{1}{2}\right)\right]\\
\quad-\frac{\Delta t}{\Delta x}\left[E_y^{n+1/2}\left(i+\frac{1}{2},j+1,k+\frac{1}{2}\right)-E_y^{n+1/2}\left(i-\frac{1}{2},j+1,k+\frac{1}{2}\right)\right]
\end{cases}
\tag{8}
$$

In the case of "thin" gratings, the regular interferogram is formed at the certain distance from the output plane of PDG. In other words, there exists a transitional area where the interferogram's space period differs from that of the master PDG. Indeed, the summation of the diffracted secondary waves with the same polarization vectors occurs at a certain time for the space overlapping. That time does actually define the extent of the transitional area.

For the gratings with a diffraction efficiency of ~100%, the PDG's thickness $L = \Lambda = \lambda_0/2\Delta n$, where $\Delta n = (n_e - n_o)$ and $n_e$, $n_o$ are the extraordinary and ordinary refractive indices, respectively [1]. For the modeling medium $n_e = 1.7$, $n_o = 1.55$, and $\Delta n = 0.15$.

In order to investigate to what extent the transitional area depends on the ratio $L/\Lambda$, the simulations were performed for PDGs with $L = \Lambda = \lambda_0/2\Delta n = 1.08\,\mu$m and the thickness equal to $\Lambda$, and $\frac{\Lambda}{3}$. The grating's size along $x$axis was $5\Lambda$.

Let's consider the calculations results according to (5), (7), (8) for the case where the linearly polarized light $(0, E_y, 0)$ falls normally to the grating of thickness $L = \lambda_0/2\Delta n = 1.08\,\mu$m and the half-period $\Lambda = L$. 2D distribution of the diffracted field for $E_x$, $E_y$, $E_z$ components is presented on Fig. 3a, b, and c, respectively. The figure shows that the regular interference pattern with the space period corresponding to the master PDG occurs at the certain distance from the PDG's output plane. The $E_z$ component contribution is negligible compared to $E_x$, $E_y$, since for calculations, $\alpha$ is assumed to be zero (see Fig. 2 and expression (3)). Taking this fact into account, let's consider the distribution of $E_x$, $E_y$ components of the diffracted field for the different ratios $L/\Lambda$. Figure 4a, b depicts the projections of the $E_x$, $E_y$ components on the plane $(x, z)$ for the given case. Fig. 4 shows that the regular interference pattern producing the master PDG, is established at the distance of $\approx 2\,\mu$m from the master PDG's output. Also, Fig. 4 represents the propagation directions

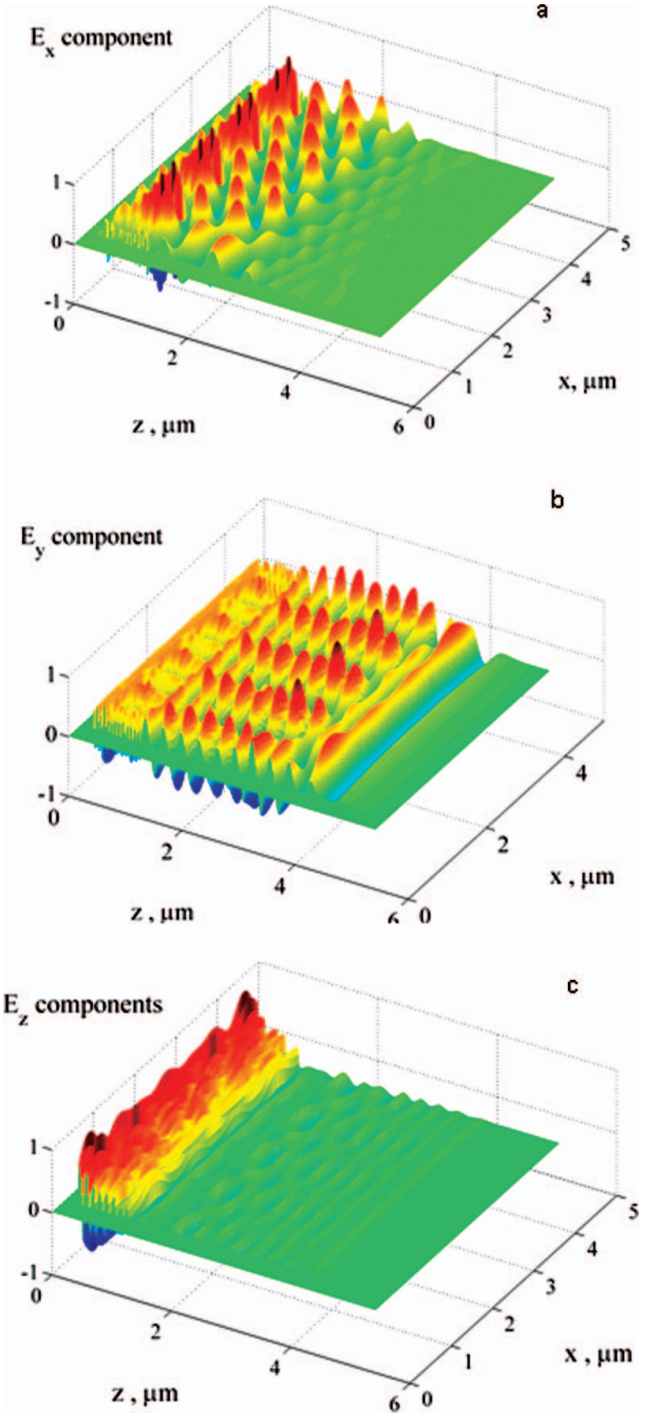


**Figure 3.** 2D distribution of diffracted field for $E_x$ (a), $E_y$ (b) and $E_z$ (c) components.

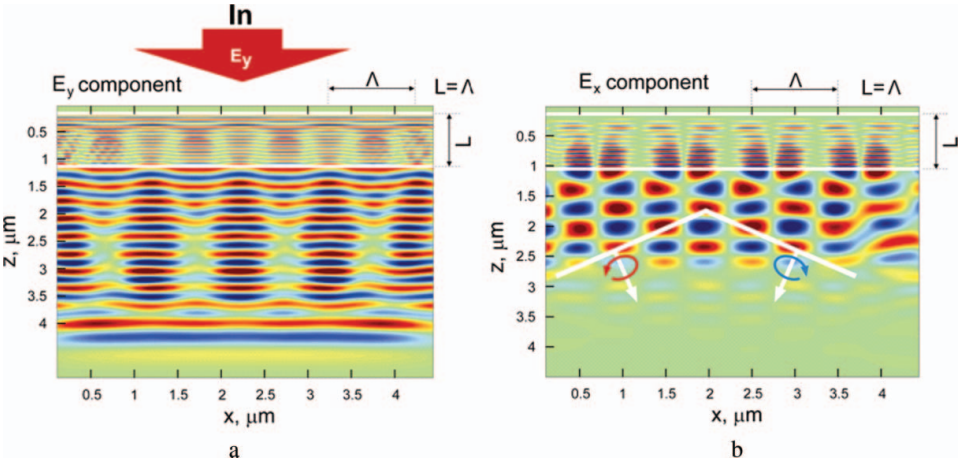


**Figure 4.** $(x, z)$ plane projections of 2D distribution of diffracted field for $E_x$ (a) and $E_y$ (b) components in the case, when $L = \Lambda = \lambda_0/2\Delta n$.

of left and right circularly polarized $-1$st and $+1$st diffracted orders. In the transitional area (at distances $< 2\,\mu$m from the master), the periodical structure of the diffracted field is not expressed well, it is rather similar to sinusoidal distribution nodes and anti-nodes.

Hence, if you position the recording replica in the transitional area, the diffraction on grating in print, besides $\pm 1$ orders, will yield to the higher orders in accordance with the nodes distribution in the plane of recording.

It is worth noting that for the chosen geometry, the behavior of the diffracted field's $E_y$ component is the most determinant of the recorded grating's parameters. Taking this fact into account, let's consider the 2D distribution of that component for the master gratings of thickness $L = \frac{\Lambda}{3} = \frac{\lambda_0}{2\Delta n}$, with a tripled period (compared to the previous case) (see Fig. 5). In such case, the transitional area is greater and equals $\approx 7\,\mu$m from the PDG's output plane.

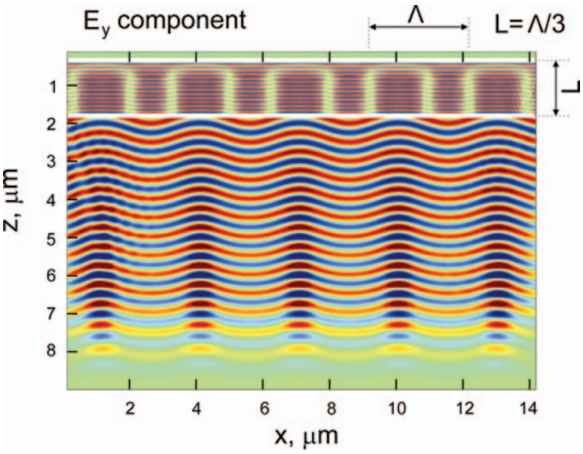


**Figure 5.** 2D distribution of diffracted field for $E_y$ component for PDGs with $L = \frac{\Lambda}{3} = \frac{\lambda_0}{2\Delta n}$.

Thus, the increase of the grating's period leads to the transitional area extension. In a real experiment, the extent of the transitional area will be greater than theoretically estimated because of the lower diffraction efficiency of the master PDG.

We conclude that at certain conditions, depending on the ratio of the master PDG's thickness to its period as well as the replica's distance from the master's output plane, the recorded grating's period differs from the master's period. The next section describes the experimental investigation of this phenomenon.

## Experiment

### *One-Dimensional Grating*

A master PDG was produced for the experiment. The polarization hologram has been written on ROLIC ROP-103 linearly photo-polymerisable polymer using two He-Cd laser (325 nm, $\approx$40 mW) beams with an orthogonal circular polarization angle between beams of $\approx 3^o$. Then the ROLIC ROF-5102 liquid crystal pre-polymer ($\Delta n = 0.15$) has been applied. The period of master grating was $2\Lambda = 6\,\mu$m, and thickness was $1\,\mu$m ($L = \frac{\Lambda}{3} = \frac{\lambda_0}{2\Delta n}$). The replica was produced by the printing method with irradiation of the master PDG by perpendicularly directed linearly polarized light of He-Cd laser. The same materials were used as an alignment layer and modulating media for master grating. The laboratory frame of reference is presented in Fig. 6. The incident light polarization vector direction $(0, E_y, 0)$ is perpendicular to the master grating's vector ($x$axis). In order to investigate how the parameters of grating in print depend on the distance from the master grating's output plane, the replica was placed at an angle to the master PDG. One end of the replica touched the master PDG, and another was 50 $\mu$m from it (Fig. 6). To ensure this distance, a 50 $\mu$m calibrated spacer was used.

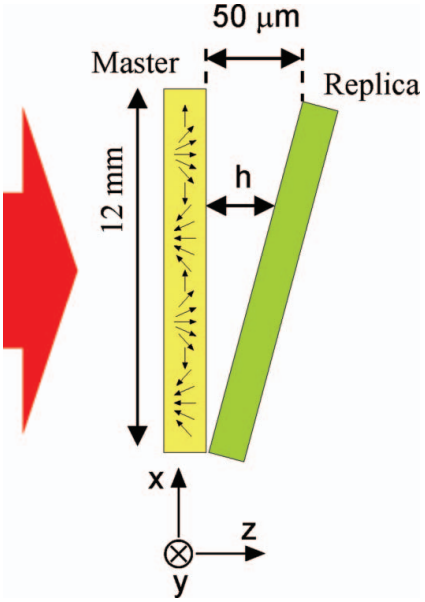


**Figure 6.** PDG printing scheme.

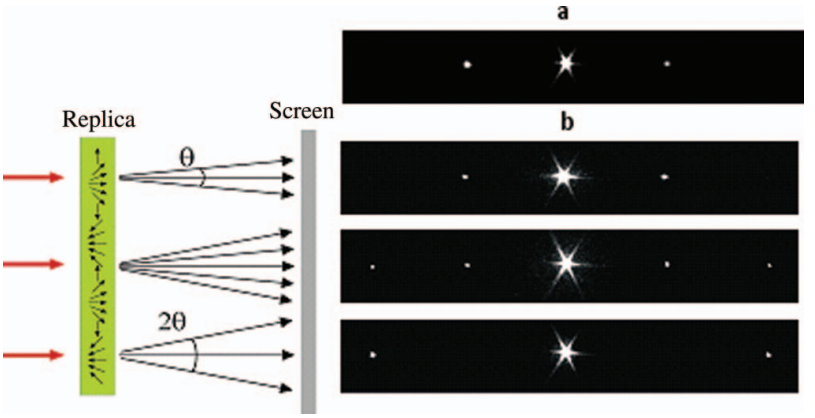


**Figure 7.** Diffraction on master – a, and printed PDG – b, (532 nm probe beam).

Figure 7a shows the diffraction on master PDG, and on Fig. 7b presents the diffraction pattern acquired by probing replica along *x*axis by a perpendicularly directed linearly polarized beam from a cw laser at 532 nm. As it can be seen on the figure, in the area where the replica was close to the master, the angular resolution is higher and corresponds to the 2nd diffraction order of the master. At the second end of the replica, the pattern reproduces the diffraction of the master. Also, there exists an area where the diffraction pattern consists of two diffracted beams corresponding to both $\pm 1$ and $\pm 2$ orders (transitional area).

Figure 8 shows the dependency of 1st and 2nd order diffraction efficiencies on the distance between master PDG and replica ($h$ is printing distance). Diffraction efficiencies were measured by probing the replica along *x*axis by a perpendicularly directed linearly polarized beam from a C.W. laser at 532 nm. At that, as $x = 0$ is considered the end of the replica, which touched the master PDG (at this point we accept $h = 0$), and on the second end of replica $x = 12\,\text{mm}$, $h = 50\,\mu\text{m}$.

For the intermediate points, $h$ was determined from the geometry, presented on the Fig. 6.

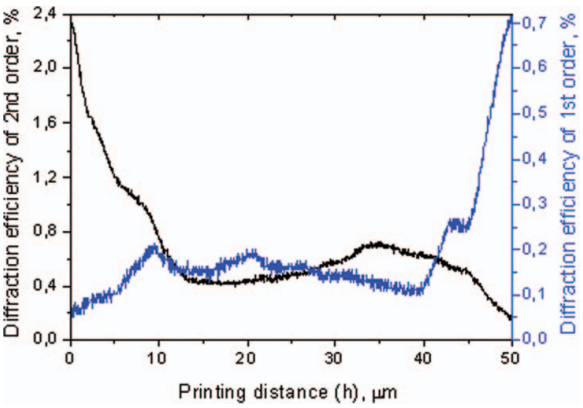


**Figure 8.**

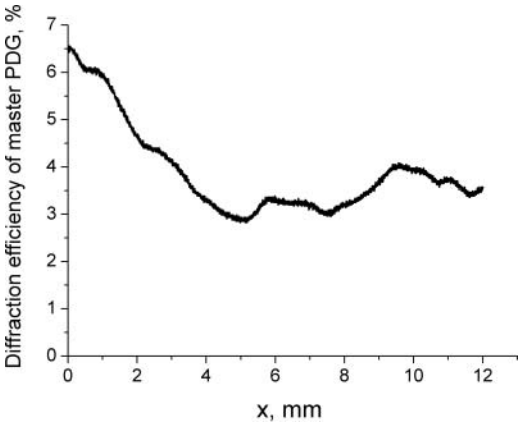


**Figure 9.** 1st order diffraction efficiency of master PDG at probing by 532 nm cw laser.

It is seen that the replica's 2nd order diffraction efficiency maximum is at $h \approx 0$. With an increase of the distance $h$ from 0 to 10 $\mu$m, the second order diffraction efficiency decreases from 2.3% to 0.55% together with an increase of the 1st-order diffraction efficiency from 0.05% to 0.2%. In the range of 10 $\mu$m $< h \leq 41$ $\mu$m, the diffraction efficiencies of 1st and 2nd orders are comparable. Then with an increase of $h$, the 1st order efficiency increases and the 2nd order efficiency decreases. Thus, according to the results of experiment (Fig. 8), the extent of transitional area of the formation of the regular interferogram, corresponding to the master PDG, is approximately 40 $\mu$m. The replica's low diffraction efficiency is determined mainly by the low efficiency of the master PDG–this fact is confirmed by the change of the master PDG's 1st-order diffraction efficiency when probing it by continuous-wave laser at 532 nm along $x$ axis (Fig. 9).

### *Two-Dimensional Grating*

The dependencies described above have been also investigated for a two-dimensional polarization grating. The recording of 2D PDG was performed by the printing method by irradiation of the master PDG by two beams of a He-Cd laser at 325 nm with orthogonal circular polarization (Fig. 10). The regimes of recording are same as that described above described for master grating preparation.

In order to investigate the process, the grating recording has been accomplished at two different distances between the master and replica: 4 $\mu$m and 20 $\mu$m. The master PDG's vector ($\vec{q}_m$) was directed perpendicularly to the vector of interference pattern ($\vec{q}_r$) formed in the field of orthogonal circularly polarized beams (patterned grating). The laboratory frame of reference is presented on Fig. 11. The periods of master and patterned gratings were $2\Lambda = 6\,\mu$m, and thickness of master PDG was 1 $\mu$m ($L = \frac{\Lambda}{3} = \frac{\lambda_0}{2\Delta n}$).

Figure 12 shows the replica's diffraction pattern recorded at distance of 4 $\mu$m from the master PDG, obtained by irradiation of a continuous wave laser at 532 nm. As is shown, the diffraction pattern is asymmetric, and diffracted beams are observed in the orders of: (1,1), (2,1), (−1, −1), (−2, −1), (2,0), (−2,0), and the diffraction efficiencies in (2,1) and (−2, −1) orders are dominant. This result can be interpreted as follows: if the angular resolution increase along $\vec{q}_m$ (the appearance of 2nd order) is determined by the replica's positioning in the transitional area of the interferogram formed at the output of the master grating, then

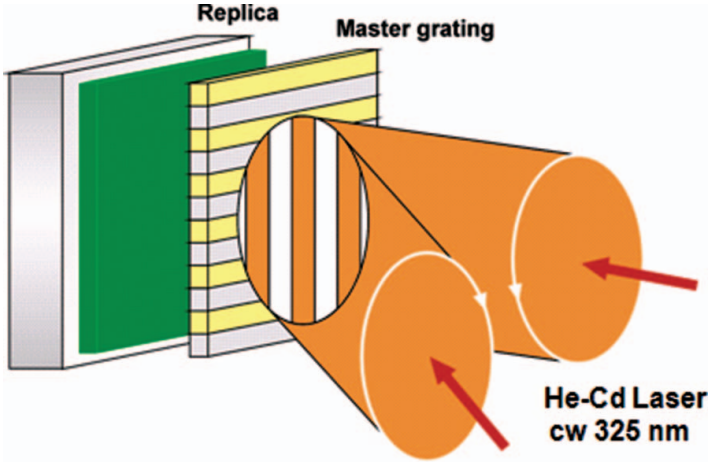


**Figure 10.** 2D PDG printing scheme.

the angular resolution along $\vec{q}_r$ (corresponding to the 1st order) is defined by the period of patterned grating only.

The diffraction pattern obtained by probing the grating recorded at distance of 20 $\mu$m from the master PDG is shown at Fig. 13. In this case the pattern is symmetric, and maximums are observed in (1,0), (−1,0), (0, −1) and (0,1) orders with the diffraction efficiencies are being dominant compared to other orders. The difference with the previous case is the absence of the angular resolution increase along $\vec{q}_m$, since in the process of recording the replica was located outside of the transitional area.

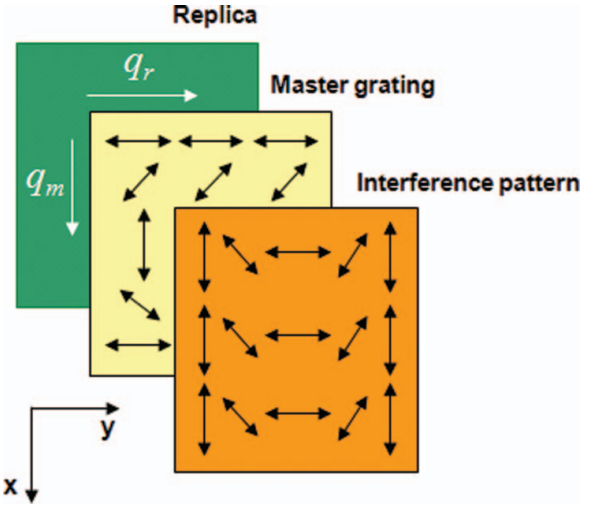


**Figure 11.** The orientations of gratings vectors.

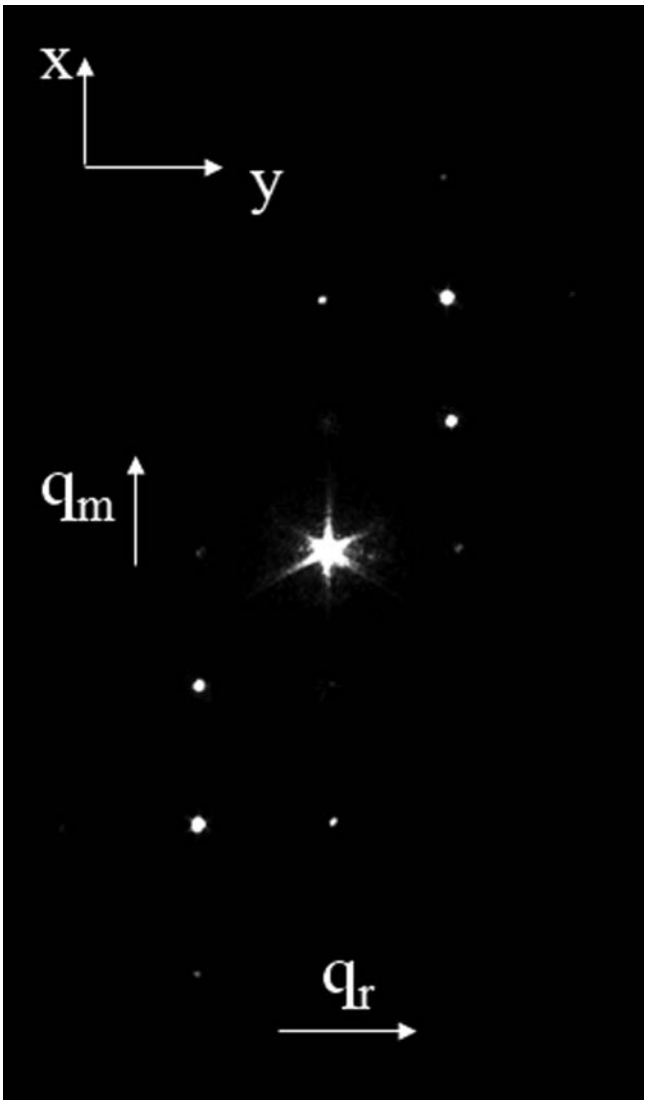


**Figure 12.** Diffraction pattern of PDG printed at distance of 4 $\mu$m from the master (532 nm probe beam).



## Discussion

This paper presented both the theoretical and experimental investigation of the effect of transitional area of an interferogram formation upon the parameters of polarization diffraction grating recorded by printing method. Particularly, it has theoretically deducted that in the transitional area the nodes/anti-nodes periods are different compared to other areas. Hence, the period of the recorded grating is determined by its location. The theoretical estimation of the transitional area extension for the master grating with thickness $L = 1\ \mu$m and half-period $\Lambda = 3\ \mu$m ($L = \frac{\Lambda}{3} = \frac{\lambda_0}{2\Delta n}$) is approximately 7 $\mu$m. The experimental results have shown that the gratings recorded at small distance from the master (4 $\mu$m)

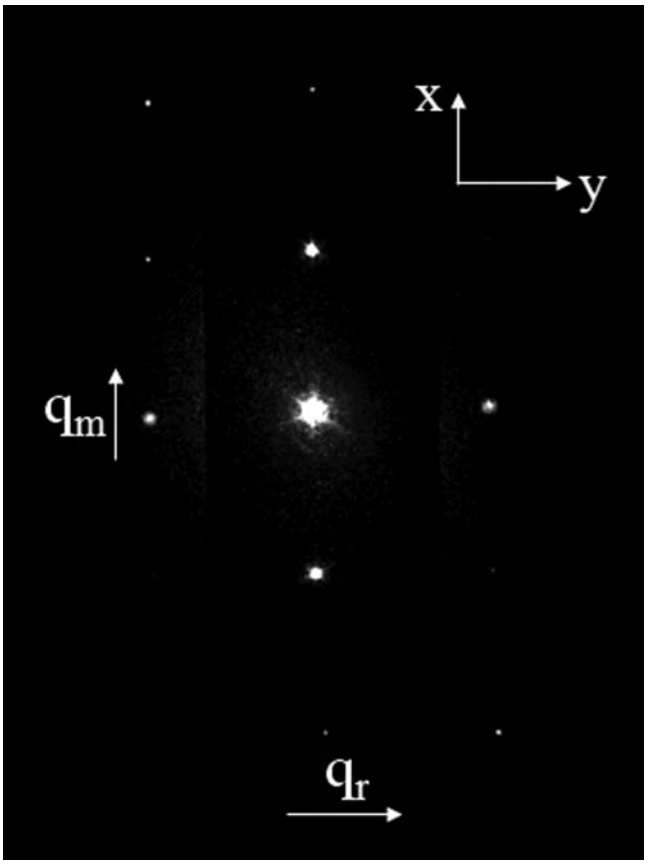


**Figure 13.** Diffraction pattern of PDG printed at distance of 20 $\mu$m from the master (532 nm probe beam).

have a period that is twice as small, and in the case where the replica is located outside of transitional area (40 $\mu$m from the master), its period reproduces the master's one. The slight mismatch between the theoretically estimated transitional area's extension and the experimental results is determined mainly by the non-ideal master grating.

The observed regularity is more evident in the case of two-dimensional polarization diffraction grating recorded by the by printing method.

The authors are confident that the obtained results can be applicable in the research and fabrication of space-chirped PDGs, as well as anisotropic two-dimensional gratings.

## Acknowledgment

This work is implemented in the frameworks of GIPP/ISTC A-1484 Project.

## References

[1] Gori, F. (1999). *J. Opt. Lett.*, *24*, 584–586.
[2] Yu, Z., Deshpande, P., Wu, W., Wang, J., & Chou, S. Y. (2000). *J. Appl. Phys. Lett.*, *77*, 927.
[3] Piquero, G., Borghi, R., & Santarsiero M. (2001). *J. Opt. Soc. Am. A*, *18*, 1339.

[4] Tervo, J., & Turunen, J. (2001). *J. Opt. Commun.*, *190*, 51.
[5] Davis, J. A., Adachi, J., Fernandez-Pousa, C. R., & Moreno, I. (2001). *J. Opt. Lett.*, *26*, 587.
[6] Hasman, E., Bomzon, Z., Niv, A., Biener, G., & Kleiner, V. (2002). *J. Opt. Commun.*, *209*, 45.
[7] Tabiryan, N. V., Nersisyan, S. R., Steeves, D. M., & Kimball, B. R. (2010). *OPN Optics & Photonics News*, *March*, p. 41.
[8] Toralf Scharf. (2007). *Polarized Light in Liquid Crystals and Polymers*, John Wiley & Sons, Inc.
[9] Jean-Pierre Bérenger. (2007). *Perfectly Matched Layer (PML) for Computational Electromagnetics*, Morgan & Claypool Publishers.
[10] Hiroshi Ono, Takuya Sekiguchi, Akira Emoto, & Nobuhiro Kawatsuki. (2008). *Japanese Journal of Applied Physics*, *47*, 3559.